ORIGINAL ARTICLE

Rho-kinase inhibition by fasudil modulates pre-synaptic vesicle dynamics

Kim Ann Saal[1,2] [ID] | Carmina Warth Pérez Arias[2,3] | Anna-Elisa Roser[2,4] |
Jan Christoph Koch[2] | Mathias Bähr[2,4] | Silvio O. Rizzoli[1,3] | Paul Lingor[2,3,4,5]

[1]Department of Neurophysiology, University Medical Center Göttingen, Göttingen, Germany

[2]Department of Neurology, University Medical Center Göttingen, Göttingen, Germany

[3]DFG Cluster of Excellence Nanoscale Microscopy and Molecular Physiology of the Brain (CNMPB), Göttingen, Germany

[4]Center for Biostructural Imaging of Neurodegeneration (BIN), Göttingen, Germany

[5]Department of Neurology, Rechts der Isar Hospital of the Technical University Munich, Munich, Germany

Correspondence
Kim Ann Saal, Department of Neurophysiology, University Medical Center Göttingen, Humboldtallee 23, 37073 Göttingen, Germany.
Email: kim-ann.saal@med.uni-goettingen.de

Funding information
Deutsche Forschungsgemeinschaft, Grant/Award Number: SFB1286/B09 and SFB1286/Z03

Abstract

The Rho kinase (ROCK) signaling pathway is an attractive therapeutic target in neurodegeneration since it has been linked to the prevention of neuronal death and neurite regeneration. The isoquinoline derivative fasudil is a potent ROCK inhibitor, which is already approved for chronic clinical treatment in humans. However, the effects of chronic fasudil treatments on neuronal function are still unknown. We analyzed here chronic fasudil treatment in primary rat hippocampal cultures. Neurons were stimulated with 20 Hz field stimulation and we investigated pre-synaptic mechanisms and parameters regulating synaptic transmission after fasudil treatment by super resolution stimulated emission depletion (STED) microscopy, live-cell fluorescence imaging, and western blotting. Fasudil did not affect basic synaptic function or the amount of several synaptic proteins, but it altered the chronic dynamics of the synaptic vesicles. Fasudil reduced the proportion of the actively recycling vesicles, and shortened the vesicle lifetime, resulting overall in a reduction of the synaptic response upon stimulation. We conclude that fasudil does not alter synaptic structure, accelerates vesicle turnover, and decreases the number of released vesicles. This broadens the known spectrum of effects of this drug, and suggests new potential clinical uses.

KEYWORDS

fasudil, recycling, ROCK, synapse, synaptic vesicle

1 | INTRODUCTION

Many neurodegenerative disorders are characterized by subclinical progression of pathology, and only become apparent when substantial damage to the nervous system has occurred. For example, in Parkinson's disease more than 50% of the nigrostriatal projections is already degenerated when the patients first present motor symptoms (Burke & O'Malley, 2013), and the disease had been developing for many years, as revealed by early non-motor symptoms as REM sleep behavior disorder or hyposmia (Chaudhuri et al., 2006; Lee & Koh, 2015). Synaptic dysfunction is known to play a critical role in numerous neurodegenerative pathologies (Schulz-Schaeffer, 2010; Spronsen & Hoogenraad, 2010; Wishart et al., 2006), and is an early event, predating the loss of neuronal projections. However, most pathology investigations are only performed at late stages, when neuronal damage and synapse loss are already evident (Bereczki et al., 2018; Pienaar et al., 2012), which limits our understanding of early neurodegeneration events, and thereby affects our ability to treat them.

Early degenerative processes may be attenuated by drugs that modulate neurite and/or synapse stability. A prominent example is a family of drugs that targets the Rho-kinase (ROCK) pathway, whose inhibition has been studied in multiple models of neurological disorders (Koch et al., 2018; Tönges et al., 2011). The ROCK pathway is involved in the regulation of actin cytoskeleton stability, and as such is an important modulator of growth cone stability, axonal growth, and regeneration (Amano et al., 1997; Endo et al., 2003; Tönges et al., 2011). More recently, ROCK signaling has also been implicated in the modulation of neuronal survival via PTEN/Akt/mTOR and autophagy (Endo et al., 2003; Guertin & Sabatini, 2007; Koch et al., 2014; Park et al., 2011; Saal et al., 2015). ROCK therefore appears to be active not only in neuronal development, but also in neuronal degeneration. It has been shown to be up-regulated in several neuropathological conditions, such as amyotrophic lateral sclerosis, multiple sclerosis, Parkinson's disease, as well as in aging, which suggests that this pathway may contribute to the etiology of neurodegeneration (Chen et al., 2015; Komagome et al., 2000; Saal et al., 2016). Similarly, an up-regulation of ROCK was shown in Alzheimer´s disease (AD) patients (Herskowitz et al., 2013). Several studies have established a connection between ROCK and Aβ production as well as clearance (Henderson et al., 2017; Lane et al., 2010). Many experimental paradigms, including mouse models of neurotraumatic and neurodegenerative disorders, have been therefore used to evaluate the effects of ROCK inhibition, for example, using the well-characterized isoquinoline derivative fasudil, a potent ROCK inhibitor. This drug improved neuronal survival and regeneration, which contributed to improved behavioral outcomes and/or survival (Bowerman et al., 2012; Günther et al., 2014; Lingor et al., 2007; Takata et al., 2013; Tatenhorst et al., 2014; Tönges et al., 2012). Additionally, ROCK inhibition not only resulted in beneficial effects on neurons, but also on astrocytes and microglia (Barcia et al., 2012; Lau et al., 2012; Monnier et al., 2003). Fasudil is licensed for human use for the treatment of subarachnoid hemorrhage in Japan and China. Clinical data from post-marketing trials and evidence in more than two decades of clinical use suggest a beneficial safety profile of the substance (Mueller et al., 2005; Shibuya et al., 1992; Shimokawa et al., 2002) and therefore render it an excellent candidate for translational clinical trials.

Since synaptic pathology is an early step in the pathogenesis of neurodegenerative disorders, and since ROCK inhibition may represent a future therapeutic option, it is imperative to test the fashion in which ROCK inhibition affects synaptic function. A major concern is that chronic treatment with ROCK inhibitors may cause substantial problems with synaptic transmission, since ROCK affects actin remodeling (Gallo, 2010), which is involved both in synaptic exo- and in endocytosis (Morales et al., 2000; Rizzoli, 2014; Sakaba & Neher, 2003). We therefore analyzed here the effects of ROCK inhibition on synaptic transmission, employing a common model for studies of synaptic and neuronal function, rat hippocampal neurons in culture. We treated the cultures with concentrations of fasudil that showed the highest effects on neuronal regeneration in vitro (Lingor et al., 2007), for several days. We observed no major effects on synaptic morphology or on basic synaptic function, although fasudil, as expected, resulted in a mild perturbation of actin organization. However, fasudil changed the proportion of synaptic vesicles that respond to stimulation, and altered the lifetime of the vesicles. This implies that chronic ROCK inhibition has moderate, but significant, effects on synaptic transmission.

2 | MATERIALS AND METHODS

2.1 | Hippocampal culture and chronic fasudil treatment

All primary neurons used for this study were obtained from 70 newborn Wistar rats of mixed gender (P0-P1), which were bred in the animal facility of the University Medical Center Göttingen. All experiments were approved by the local authority, the Lower Saxony State Office for Consumer Protection and Food Safety (Niedersächsisches Landesamt für Verbraucherschutz und Lebensmittelsicherheit) under the license number T10/28.

Dissection of hippocampi from the rat brains was performed as described before (Opazo et al., 2010; Truckenbrodt et al., 2018). Briefly, pups were decapitated, brains were extracted, hippocampi were dissected and collected in HBSS (Cat. no. #14175-053, Invitrogen). Tissue pieces were digested with an enzyme solution (10 ml DMEM (Cat. no. D5671, Merck), 2 mg cysteine (Cat. no. #30090, Merck), 100 mM $CaCl_2$ (Cat. no. #102382, Merck), 50 mM EDTA (Cat. no. #108418, Merck), and 25 U papain (Cat. no. #LS003126, Worthington)) for 1 hr. Enzyme activity was stopped by an inactivating solution (10 ml FCS-containing DMEM (FCS Cat. no. #S0615, Merck) and 4 mg BSA (Cat. no. #A1391, Applichem, Darmstadt, Germany)) for 15 min. Cells were

mechanically dissociated by trituration and seeded at a density of 30,000 cells/cm^2 on poly-L-lysine-coated (PLL, Cat. no. #P2658, Merck) glass coverslips or 6-well plates for western blotting into plating medium (DMEM supplemented with 10% horse serum (Cat. no. #S900-500, VWR International GmbH, Darmstadt, Germany), 3.3 mM glucose (Cat. no. #108342, Merck), and 2 mM glutamine (Cat. no. #25030-024, ThermoFisher Scientific). They were kept at 37°C and 5% CO$_2$ and medium change was performed 1–4 hr after plating to Neurobasal culture medium (Neurobasal-A medium (Cat. no. #10888-022) containing 1:50 B27 supplement (Cat. no. #17504-044) and 1:100 GlutaMAX (Cat. no. #35050-038), all ThermoFisher Scientific). Neurons were cultured for up to 15 days in vitro (DIV). Five days before starting any of the experiments explained below, cells were treated with 20 μM fasudil (Cat. no. #F-4660, LC Laboratories), by adding it into the culture medium. As we had shown previously, a concentration of 20 μM fasudil was most effective in paradigms of neuronal protection and neurite outgrowth in acute neurodegenerative in vitro models (Lingor et al., 2007; Tönges et al., 2012). To evaluate chronic effects of fasudil on pre-synapses we used the same concentration and incubated the neurons for 5 consecutive days. Fasudil was replenished on the third day of treatment (DIV12), by adding the double amount of fresh medium containing 20 μM fasudil to the existing medium. Each experiment was carried out after 5 consecutive days of fasudil treatment.

2.2 | Actin purification and western blot analysis of G-actin

To test the effects of fasudil on the actin cytoskeleton, neurons were collected and a western blot analysis for globular actin (G-actin) and filamentous actin (F-actin) was performed, using a G-actin/F-actin assay kit (Cat. no. #BK037, Cytoskeleton Inc.) according to manufacturer´s instructions. In brief, neurons were harvested in a lysis buffer that stabilizes F-actin, containing 100 mM ATP and proteases inhibitors. Cells were then centrifuged at 350 *g* at 23°C room temperature to pellet unbroken cells and fragments. The supernatant was ultracentrifuged at 100,000 *g* at 37°C for 1 hr, to separate F-actin from G-actin. F-Actin was then depolymerized, and actin amounts were assessed by SDS page. As positive controls, actin standards of 10, 20, and 50 ng were loaded to the gel to estimate the actin amount in the samples. Protein was transferred to a nitrocellulose membrane, blocked with 5% non-fat milk (Cat. no. #A0830, Applichem) in TBS-T (200 mM Tris-base (Cat. no. #108382, Merck, 1.3 M NaCl (Cat. no. #567440, Merck), 1% Tween 20 (Cat. no. #8221840500, Merck)), and was incubated with polyclonal rabbit anti-G-actin antibodies (G-actin/F-actin assay kit), for 1 hr at 23°C room temperature. Horseraddish peroxidase (HRP)-coupled secondary anti-rabbit antibodies (RRID:AB_2099233, Cell Signalling Technologies) were added for 0.5 hr, and were finally treated with enhanced chemiluminescence reagents (ECL™Prime Western-Blot-System Cytiva kit, Cat. no. #GERPN2232, Merck) to visualize the G-actin bands. By calculating the ratio of G- and F-actin for each condition, fasudil effects on the filamentous actin cytoskeleton can be quantified.

2.3 | Electrical field stimulation

All experiments for the investigation of chronic fasudil treatment on stimulated hippocampal neurons were performed by placing the living neurons in a custom-made stimulation chamber in 37°C physiological Tyrode buffer (124 mM NaCl, 5 mM KCl Cat. no. # 104,936, Merck), 30 mM glucose, 25 mM 2'[4-(2'hydroxyethyl)-1-piperazinyl]-ethanesulfinicacid (HEPES, Cat. no. #110110, Merck), 2 mM CaCl2, 1 mM MgCl2 (Cat. no. #105833, Merck), pH 7.4). Electrical field stimulation was then applied in pulses of 20 Hz for 30 s, at 100 mA, with a stimulus isolator and an Accupulser stimulator (World Precision Instruments, Friedberg, Germany) at 23°C room temperature. Neurons were left in buffer and fixed with 4% paraformaldehyde (PFA, Cat. no. #P6148, Merck). As unstimulated controls, neurons were incubated in pre-cooled Tyrode buffer (4°C) containing 3 μM tetrodotoxin (TTX, Cat. no. 1069/1,Tocris Bioscience, Bristol, UK) at 4°C for the respective time and fixed with 4% PFA.

2.4 | Western blot analysis of synaptic proteins

Fasudil-treated and vehicle-treated control hippocampal neurons were separately collected on ice in RIPA lysis buffer (Cat. no. #89900, Thermo Scientific), including complete protease inhibitor cocktail (Cat. no. #04693116001, Merck) and phosphatase inhibitors (PhosSTOP, Cat. no. #04906845001, Merck). Cell lysates were sonicated, protein amount was quantified by a BCA protein assay (Cat. no. #23225, Thermo Scientific), and dithiothreitol (Cat. no. #43815, Merck) was added. In a 12% gel, 20–30 μg protein were loaded and separated by SDS page. After electroblotting to a nitrocellulose membrane in blotting buffer (250 mM tris-base, 1.9 M Glycine (Cat. no. #1042011000, Merck), 20% Methanol (Cat. no. #1060092500, Merck)), proteins were blocked with 5% non-fat milk in TBS-T, and were incubated with the following primary antibodies in TBS-T buffer overnight at 4°C: rabbit polyclonal anti-synapsin1 (RRID: AB_2721082), rabbit polyclonal anti-VAMP1 (vesicle-associated membrane protein1, RRID: AB_887807), rabbit polyclonal anti-VAMP2 (vesicle-associated membrane protein2, RRID: AB_887811), rabbit polyclonal anti-synaptophysin1 (RRID: AB_1210382), rabbit polyclonal anti-SV2A (synaptic vesicle glycoprotein2A, RRID: AAB_2721088), mouse monoclonal anti-synaptotagmin1 (RRID: AB_887835; all from Synaptic Systems, Göttingen, Germany), rabbit polyclonal anti-phospho-synapsin1 (RRID: AB_10002135, specific for pSer549, Novus Biologicals, Centennial, USA) and rabbit polyclonal anti-GAPDH (RRID: AB_796208, Sigma, now Merck, Darmstadt, Germany). Between primary and secondary antibody incubations, membranes were washed with TBS-T. HRP-coupled secondary antibodies (anti-mouse HRP, RRID: AB_330924; anti-rabbit

HRP, RRID:AB_2099233, Cell Signalling Technologies) were applied for 1 hr at 23°C room temperature in TBS-T buffer. Protein bands were visualized using an ECL-solution kit and all band intensities were analyzed using ImageJ (N.I.H., Bethesda). For better visualization of the bands in Figure 2 the brightness and contrast were scaled.

2.5 | Live-cell experiments and the respective data analysis

To investigate synaptic vesicle dynamics after chronic fasudil treatment, neurons were placed into the stimulation chamber with pre-warmed Tyrode buffer containing a monoclonal antibody against the luminal domain of synaptotagmin1 (Syt1, RRID: AB_10547969, Synaptic Systems) conjugated to the fluorophore Atto647N. Electrical field stimulation was applied after 30 s in pulses of 20 Hz for 30 s. Neurons were left in the antibody solution for further 5 min, to enable them to complete transmitter release and endocytosis of the synaptic vesicles. As unstimulated control, neurons were incubated with the Syt1 antibody in the presence of 3 μM TTX at 4°C for 6.5 min, to suppress spontaneous activity and transmitter release. Afterwards neurons were washed with Tyrode buffer and fixed for further immunocytochemistry (ICC).

To evaluate the synaptic vesicle kinetics, neurons were incubated with Syt1 antibodies conjugated with the pH-sensitive dye CypHer5E (RRID: AB_2199307, Synaptic Systems) for 1hr at 37°C. After washing the cells with Tyrode buffer, electrical field stimulation (20 Hz for 30 s) was applied to trigger transmitter release. Changes in CypHer5E fluorescence were recorded with an epifluorescence microscope every two seconds for 360 s.

The CypHer5E fluorescence over time was analyzed with the ImageJ plugin "intensity versus time monitor". A bleaching and shift correction was calculated and applied with Matlab (The Mathworks Inc.). The fluorescence intensity for each time frame was averaged, depicting a curve of fluorescence change after stimulation. The measured fluorescent signal decreased during exocytosis, as CypHer5E is exposed to the neutral extracellular pH, which quenches the dye, and increased during endocytosis, as the pH luminal milieu decreased through the acidification of the vesicles, thereby activating the CypHer5E fluorescence. The exocytosis and endocytosis signals were fit to single exponential curves, which provided the time constants (τ) for both exo- and endocytosis. Using these calculations, the vesicle kinetics for exocytosis and endocytosis were compared between the control and the fasudil-treated group, and were depicted as means per condition.

2.6 | Neuronal activity evaluation using the calcium indicator construct GCaMP6s

Cells were co-transfected on DIV4 with GCaMP6s and a chimeric pH-sensitive mOrange2, which was cloned into rat synaptophysin1

(Truckenbrodt et al., 2018) to identify vesicle-releasing synapses, named SypHy. Transfections were performed with a standard calcium phosphate kit (Cat. no. #E1200, Promega), used as previously described (Truckenbrodt et al., 2018). The fasudil treatment started on the same day. The GCaMP6s fluorescence signal was recorded in the living neurons on DIV 8 with an epifluorescent microscope for 240 s. This procedure depicts the calcium influx in the neurons, and therefore the neuronal activity. At 60, 90, and 120 s after starting the recording the cells were electrically stimulated with 20 Hz for different durations (1 s, 10 s, and 50 s), and GCamp6s fluorescent intensity was analyzed with a Matlab written routine, using the SypHy fluorescence signal to identify synaptic boutons. The maximal GCamp6s fluorescence intensity generated by each stimulus was assessed and the area under the curve (AUC) was calculated using the Riemann sum paradigm.

2.7 | Analysis of chronic changes in vesicle turnover

For the assessment of changes in vesicle turnover after chronic fasudil treatment, cultures were again exposed to Syt1 antibodies conjugated to Atto647N, as described in Truckenbrodt et al., 2018 (Truckenbrodt et al., 2018). Briefly, neurons were incubated with the antibodies at DIV11 (1 day after starting with fasudil treatment), for 1 hr at 37°C. The antibody is endocytosed in vesicles that recycle during the spontaneous network activity of the neurons. During this treatment, the entire recycling pool of synaptic vesicles is labeled. The vesicles afterward age, and are eventually degraded (Truckenbrodt et al., 2018), thereby disappearing from the synapses. To compare the vesicle aging of fasudil-treated neurons with that taking place in control cultures, neurons were fixed at different time points after antibody incubation. The first cells were fixed 2 hr after antibody incubation (DIV11), to indicate the initial vesicle population in both treatments. Other fixation points were performed at every 24 hr after the initial treatment (DIV12-DIV15). All neurons were additionally stained after fixation with antibodies for synaptophysin1, to identify the synaptic boutons and imaged confocally. Vesicle turnover was estimated for each day by measuring the Syt1-Atto647N fluorescence intensity persisting in the synaptophysin1-identified synapses using a custom-written Matlab routine. Means per DIV were normalized to the initial Syt1 fluorescence intensity (DIV11) and were compared by combining the decrease in fluorescence over all DIV (DIV12-15) for fasudil-treated and untreated neurons, respectively.

2.8 | Cell fixation and immunocytochemistry

Fasudil-treated neurons and controls were fixed with 4% PFA in PBS for 10 min at 4°C, and for further 30 min at 23°C room temperature. Then, cells were briefly washed with PBS and quenched with 100 mM NH_4Cl (Cat. no. # 101145100, Merck) for 20 min at 23°C room temperature. Permeabilization and blocking were performed

using 0.1% TritonX-100 (Cat no. #1122980100, Merck) and 2.5% BSA in PBS, exchanging the solution two times, each for 5 min. Primary antibodies were diluted in the blocking solution, and cells were incubated for 1 hr at 23°C room temperature, in a wet chamber.

We relied on primary rabbit or guinea pig polyclonal anti-synaptophysin1 antibodies (guinea pig, RRID: AB_1210382, Synaptic Systems) which were revealed with a secondary AlexaFluor488 antibody (anti-rabbit AF488, RRID: AB_2340620; anti-guinea pig AF488, RRID: AB_2337440 Dianova, Hamburg, Germany) for identifying the pre-synaptic compartment in all fixed samples. For the evaluation of actin localization in the synapse with STED microscopy (Figure 1b), cells were additionally stained with rhodamine phalloidin (R415, RRID: AB_2572408, Invitrogen), or monoclonal mouse anti-ß-actin (RRID: AB_476697 Sigma, now Merck), revealed with a secondary Atto647N anti-mouse antibody (Cat. no.: #50185-1Ml-F, Sigma, now Merck). Here, synaptophysin1 was detected with secondary Chromeo494 anti-mouse antibodies (Cat no. #15032, Active Motif).

To scrutinize the effects of fasudil on the actin cytoskeleton and on downstream targets of ROCK after electrical stimulation, immunocytochemistry was performed for F-actin (phalloidin-Atto647N, Cat. no. #65906, Sigma, now Merck), ß-actin, phospho-myosin regulatory light chain (pMRLC, RRID: AB_2250969, Cell Signaling Technologies), and phospho-cofilin (pCofilin, Cat. no. #3313T, Cell Signaling Technologies). All primary antibodies were detected by nanobodies conjugated to Star635P (FlouTag®-X2 anti-mouse IgG, Cat. no. #N2002-Ab635P-S; FluoTag®-X4 anti-rabbit IgG, Cat. no. #N2402-Ab635P-S, NanoTag Biotechnologies). Synapses were again identified by co-staining with synaptophysin1 and samples were imaged using STED microscopy.

For evaluation of phosphorylation of synapsin1 after fasudil treatment in the stimulation paradigm, fixed neurons were stained with either a primary antibody for synapsin1 phosphorylation site 1 (phospho-Syn9, RRID: AB_2816295, Thermo Fisher Scientific) or phosphorylation site 6 (phospho-Syn549, RRID: AB_2175503, Thermo Fisher Scientific).

For experiments investigating the chronic fasudil effect on synaptic vesicle dynamics, neurons were fixed after the live-cell experiments involving Syt1 antibodies conjugated to Atto647N, and were co-stained with a polyclonal guinea pig anti-synaptophysin1 antibody, for synapse identification.

All fixed and stained samples were embedded in Mowiol 4–88 mounting medium (Cat. no. #0713.2, Carl Roth GmbH).

2.9 | Imaging

General fluorescent microscopy and live imaging were performed with an inverted Nikon Eclipse Ti epifluorescence microscope (Nikon Corporation), equipped with a Plan Apochromat 60x, 1.4 NA oil-immersion objective, a HBO-100W Lamp, and an IXON X3897 Andor camera. For confocal and STED imaging of actin distribution (Figure 1b), synaptotagmin1-Atto647N uptake into synaptic

vesicles after electrical stimulation (Figure 3), and vesicle turnover, a Leica Ti-E STED TCS SP5 microscope (Leica Microsystems) was used, equipped with pulsed diode lasers with 640 nm emission for excitation of Atto647 and with 531 nm emission for excitation of Chromeo494 (both from PicoQuant). For depletion of Atto647 and Chromeo494, a pulsed infrared titanium:sapphire (Ti:Sa) tunable laser (1W, 80 MHz, 720–1,000 nm, Mai Tai Broadband; Spectra-Physics) was used, set at a wavelength of 750 nm. Confocal imaging was performed using an Argon laser to excite Alexa488 and a HeNe laser line (633 nm) for excitation of Atto647. The detectors used were ultra-sensitive avalanche photodiodes and high-sensitivity, low-noise PMTs (Leica). All scans were acquired with a 100 × HCX PL APO oil-immersion STED objective (NA 1.4), using the Leica LAS AF imaging software, with a pixel size of 20 × 20 nm and a scanning speed of 1 kHz.

For the analysis of fasudil effects on different ROCK downstream effectors (Figure 1d and e) and phosphorylation states of synapsin1 (Figure 2d and e) confocal and STED images were generated by employing a multicolor microscope setup (Abberior Instruments) based on an IX83 microscope (Olympus) equipped with an UPLSAPO 100 × 1.4 NA oil immersion objective (Olympus). To obtain confocal images of synaptophysin1-AlexaFluor488 a 485 nm excitation laser (set to 5%–15% of max. power) was employed, and signal was detected with an avalanche photodiode unit (APD) at 550/50 nm. For STED imaging the excitation of Star635P and phalloidin-Atto647N fluorophores was obtained using 640 nm laser, pulsed at 80 MHz. Depletion for fluorophores was effected by 775 nm depletion laser (set to 10%–30% of max. power of 1.2 W, depending on brightness of staining of the target proteins). Scanning was performed with a dwell time of 15 μs per pixel with 20 nm pixel size.

2.10 | Data collection and processing

From confocal and STED images, the actin distribution depending on synapse morphology was quantitatively investigated as follows: regions of interest (ROIs) were selected using the synaptophysin1 (Syp1) signal as a reference, and were centered on the Syp1 center of mass with a custom written Matlab routine. They were then rotated and aligned, based on the actin signal in the respective synapses (Figure 1c). This results in an average profile of both Syp1 and actin in the experiments, which can be easily analyzed by performing line scans across the synapses.

For changes in ROCK downstream effectors after fasudil treatment with or without electrical field stimulation, confocal images of Syp1 immunofluorescence were used to generate a mask for pre-synapse identification. Using a custom-written Matlab routine, the fluorescence signal of the target protein in the STED images was measured in the locations provided by the Syp1 immunofluorescence. The signals were normalized to the Syp1 immunofluorescence to avoid differences between cultures induced by different synapse sizes or numbers of vesicles. For each target 28–30 images from 3 to 4 independent cell culture preparations were analyzed. For the
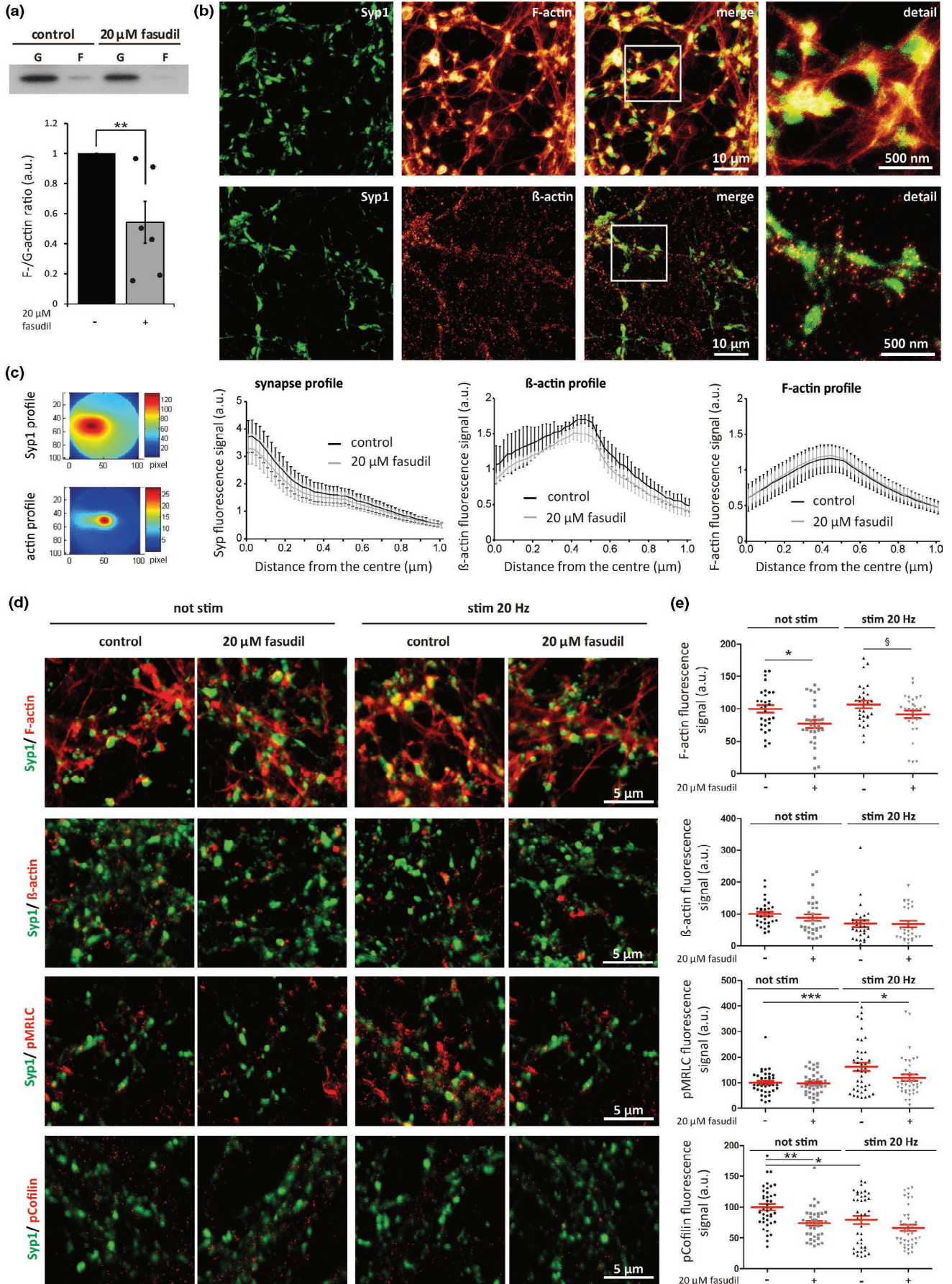
FIGURE 1 Effects of chronic fasudil treatment on ROCK downstream effectors in cultured neurons. (a) Western blot analysis shows a significant reduction of filamentous actin (F-actin) in fasudil-treated neurons (G: globular actin, F: filamentous actin). The ratio between F- and G-actin was calculated from treated and untreated cultures ($n = 6$ independent cell culture preparations and actin purifications). (b) Representative STED images of neurons either stained with phalloidin, to label specifically F-actin, or with antibodies against ß-actin. Synaptophysin1 (Syp1) identifies the presynaptic boutons. (c) All synapses from images as those in panel B were overlapped, and centered on the center-of-mass of the Syp1 spots. The synapse images were then rotated until an optimal alignment of their respective actin signals could be obtained. The color scheme shows a representative Syp1 signal for an experiment with control neurons (top), and the respective actin signal (bottom). Line scans were drawn from the center of the aligned synapses to the periphery, and were compared between controls and fasudil-treated samples. No significant differences could be observed ($n = 3$ independent cell culture preparations, with several hundred synapses analyzed per preparation). (d) Exemplary STED images of four target proteins show the influence of fasudil on the ROCK signaling pathway in 20 Hz stimulated (stim 20 Hz) and unstimulated hippocampal cultures (not stim). F-actin, ß-actin and phospho-myosin regulatory light chain (pMRLC) are shown in red, while Syp1 is shown in green (e). Quantification of presynaptic F-actin showed a significant reduction in unstimulated fasudil treated neurons and a trend towards less phalloidin staining in the stimulated condition (§: $p = .057$), when compared with not stimulated controls (all $n = 30$ images from 3 independent culture preparations with hundreds of synapses analyzed per experiment), while the ß-actin levels were unaffected (not stim ctrl $n = 30$, not stim fasudil $n = 30$, stim ctrl $n = 30$, stim fasudil $n = 28$ images from 3 independent culture preparations with hundreds of synapses analyzed per experiment). pMRLC fluorescence increased after stimulation, whereas fasudil treatment counteracted MRLC phosphorylation significantly (all $n = 40$ images from 4 independent culture preparations with hundreds of synapses analyzed per experiment). pCofilin fluorescence is strongly reduced following stimulation and significantly decreased in fasudil-treated cultures (not stim ctrl $n = 40$, not stim fasudil $n = 40$, stim ctrl $n = 38$, stim fasudil $n = 40$ images from 4 independent culture preparations). Data are presented as individual data points and/or mean $\pm$ SEM.

quantification of pCofilin, which colocalized less with the Syp1 immunofluorescence than the other markers, the overall fluorescence signal per image was calculated for both pCofilin and Syp1, rather than in the Syp1-defined masks.

2.11 | Study design

The study was not pre-registered and no randomization, blinding and sample size calculation was applied.

2.12 | Statistics

Data were collected from at least $n = 3$ independent cell culture preparations or more as stated in the legend of each figure. No test for outliers was performed. As test for normality, the Jarque-Bera-Test was applied using a Matlab-written routine. Statistical differences between fasudil-treated neurons and controls in normally distributed data were assessed using the unpaired Student´s t-test with SigmaPlot 10.0 (Systat Software GmbH), unless stated otherwise. In the case that data were not normally distributed the Mann–Whitney test was applied to test the statistical differences between the groups and stated in the respective legend. For the comparison of stimulated versus unstimulated neurons after fasudil treatment, data were normalized to synaptophysin1 signal and again normalized to the unstimulated controls without fasudil treatment. Here, a one-way ANOVA with a Bonferroni test for multiple comparisons as post hoc test was applied to ascertain significant differences between the groups with Prism Software (GraphPad Software Inc.). All data are presented as individual data points and/or means $\pm$ SEM. Differences were considered significant and indicated by asterisks with *$p < .05$; **$p < .01$; ***$p < .001$, unless stated otherwise.

2.13 | Data and material sharing statement

Upon a reasonable request, all custom-built materials and designed Matlab routines will be shared.

3 | RESULTS

3.1 | Chronic fasudil treatment changes activity of downstream ROCK effectors, but does not change actin organization in synapses

To investigate the effects of chronic treatment of the pharmacological ROCK inhibitor fasudil on synapses, primary hippocampal neurons were cultured for up to 15 DIV and chronic fasudil treatment was performed for 5 days.

For a proof-of-principle of the mechanism-of-action of fasudil, we first analyzed its influence on downstream effectors of ROCK. First, we separated the cellular actin amounts into the soluble monomeric fraction (globular or G-actin) and into the insoluble cytoskeletal fraction (filamentous or F-actin). A western blot analysis of both actin fractions revealed decreased band intensities for F-actin after fasudil treatment (Figure 1a). The fraction of F-actin in the cultures decreased significantly, presumably because of an enhanced cofilin activity, owing to ROCK inhibition (Amano et al., 1997).

Since actin is a prominent component of pre-synapses, we investigated whether the decrease in the F-actin fraction in the cultures was also accompanied by a change in the organization of actin in the synaptic bouton. We analyzed actin by super-resolution stimulated emission depletion (STED) microscopy. The distribution of F-actin was determined by phalloidin staining, while both G- and F-actin were stained with an antibody against ß-actin (Figure 1b). This provides a far less prominent staining than
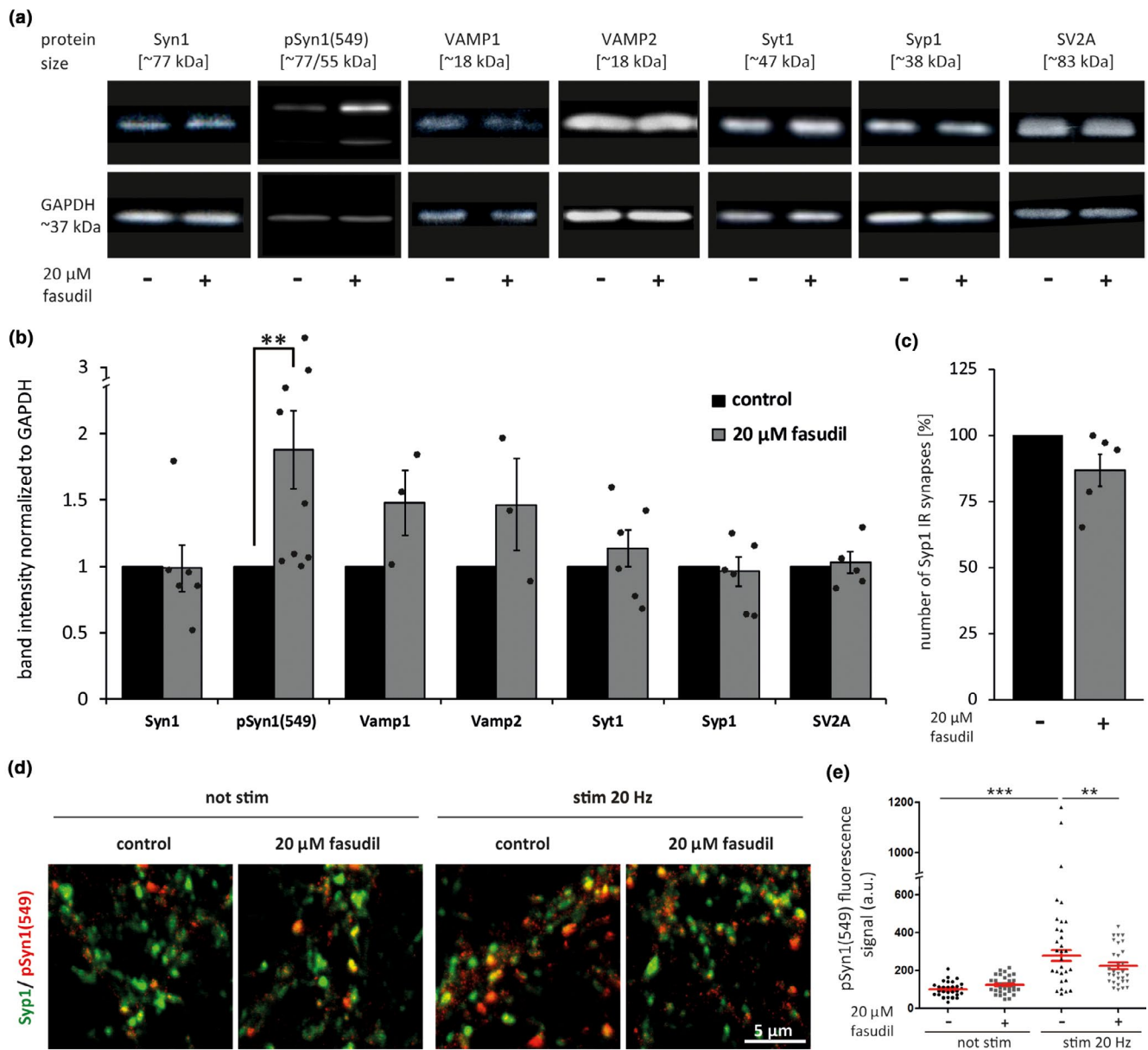
FIGURE 2 The effects of fasudil treatment on synaptic protein expression and synapsin1. phosphorylation. (a) Representative images of Western blot bands of different presynaptic proteins from fasudil-treated and vehicle-treated neuronal cultures, (b) Band quantifications reveal that fasudil does not have significant overall effects on the expression of synapsin1 (Syn1, $n = 6$ independent cell culture preparations), vesicle associated membrane protein1 (VAMP1, $n = 3$ independent cell culture preparations), vesicle associated membrane protein2 (VAMP2, $n = 3$ independent cell culture preparations), synaptotagmin1 (Syt1, $n = 6$ independent cell culture preparations), synaptophysin1 (Syp1, $n = 6$ independent cell culture preparations) and synaptic vesicle protein2A (SV2A, $n = 6$ independent cell culture preparations). When examining the phosphorylation state of synapsin1 (pSyn1(549)), fasudil treatment resulted in a pronounced increase in phosphorylation ($n = 9$ independent cell culture preparations). The immunoblot intensities were normalized to a protein not expected to change across experiments and conditions, GAPDH. The intensities of the fasudil-treated samples were then normalized to the respective controls, and were plotted. (c) Quantification of the total number of synaptophysin1 immunoreactive (Syp1 IR) synapses (see Figure 1b), failed to reveal a significant effect of the fasudil treatment ($n = 5$ independent cell culture preparations). (d and e) The phosphorylation of synapsin1 at site 6 (Syn1(549)) was increased in stimulated controls (not stim ctrl $n = 30$, stim ctrl $n = 30$ images from 3 independent culture preparations with hundreds of synapses analyzed per experiment), while its phosphorylation level was significantly reduced after fasudil treatment during stimulation ($n = 30$ images from 3 independent culture preparations with hundreds of synapses analyzed per experiment). The trend towards higher syn1(549) phosphorylation in fasudil-treated unstimulated neurons ($n = 30$ images from 3 independent culture preparations with hundreds of synapses analyzed per experiment) was not significant when compared to unstimulated controls. Data are given as individual data points and means $\pm$ SEM
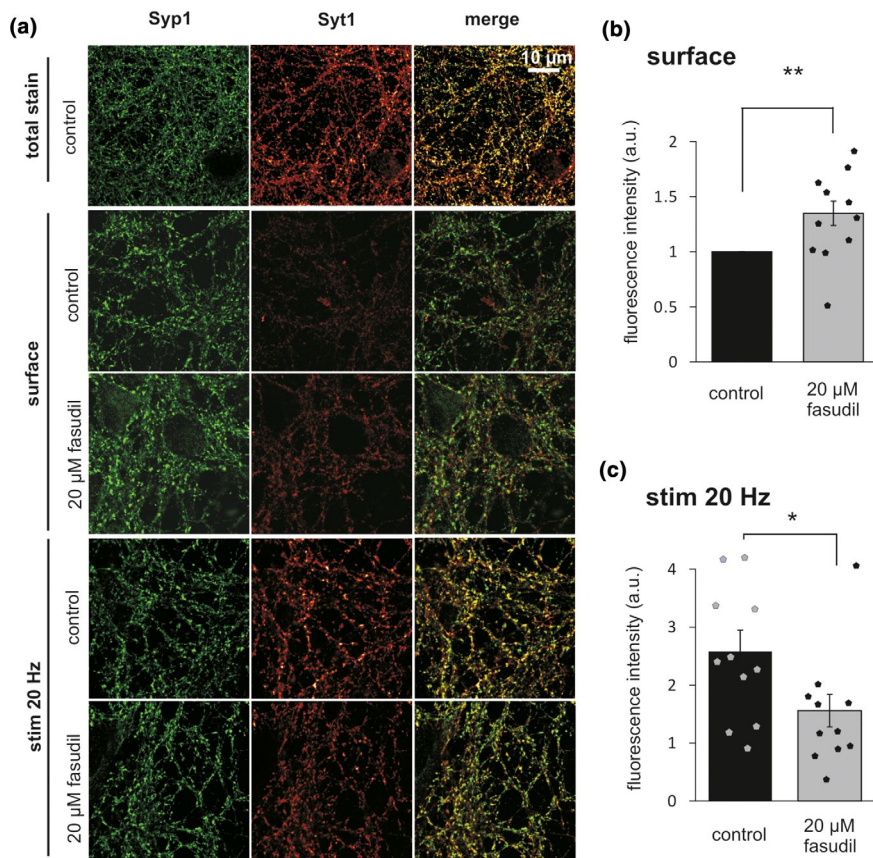
FIGURE 3 The recycling vesicle pool is reduced by fasudil treatment. (a) Representative STED images of neurons exposed to fluorescently-conjugated Syt1 antibodies in the absence of stimulation (top panels) or after stimulation for 30 s at 20 Hz. (b) An analysis of the surface population of Syt1 molecules ($n = 11$ independent cell culture preparations, with several hundred synapses analyzed per experiment). (c) A similar analysis of the vesicle population that responds to stimulation ($n = 11$ independent cell culture preparations with several hundred synapses analyzed per experiment, $*p < .05$ with Mann-Whitney Test). Syp1: synaptophysin1, Syt1: synaptotagmin1. Data are presented as individual data points and mean $\pm$ SEM

phalloidin, because of its larger size, which does not enable it to penetrate easily into synapses, but is not absolutely dependent on F-actin, as phalloidin. The pre-synaptic boutons were identified by synaptophysin1 (Syp1) staining. We observed no obvious changes after chronic fasudil treatment with a quantitative analysis of synapse morphology using the Syp1 signal as the center of mass (Figure 1c). Performing line scans across the synapses, the synapse (Syp1) profile of fasudil-treated neurons was virtually identical to that of untreated neurons (Figure 1c). We made the same observation for both actin stainings.

Actin and other downstream effectors of ROCK were investigated after chronic fasudil treatment by an electrical field stimulation paradigm. Fluorescence intensities of phalloidin, ß-actin, phospho-myosin regulatory light chain (pMRLC) and phospho-cofilin (pCofilin) stainings were quantified in stimulated and unstimulated neurons using STED imaging (Figure 1d and e). The F-actin amount was not altered by stimulation, but fasudil reduced the fluorescence signal of phalloidin significantly in the unstimulated condition, and exhibited a similar trend in the stimulated condition. ß-actin was not affected by fasudil treatment and also not by stimulation. The phosphorylation of MRLC in the pre-synapse was significantly increased because of electrical stimulation, but was not altered by the fasudil treatment. The overall amount of pCofilin was significantly reduced by stimulation (Figure 1e), and fasudil treatment reduced the signal in the unstimulated cultures compared to controls. However, this fasudil-induced reduction was not significant in stimulated cells.

These experiments confirm that chronic fasudil treatment inhibits the ROCK signaling pathway by affecting the pre-synaptic activity of MRLC and cofilin, and by changing the proportion of F-actin. In this paradigm, it did not result in major changes in synaptic morphology or actin distribution.

3.2 | Chronic fasudil treatment influences synapsin1 phosphorylation

Next to the effects of fasudil on the proteins involved in actin cytoskeleton organization, other cellular pathways are also affected by this kinase inhibitor (Davies et al., 2000; Mueller et al., 2005). To quantify the effects of fasudil on the levels of pre-synaptic proteins, we performed a western blot analysis of several pre-synaptic proteins that are involved in synaptic transmission (Figure 2a). The expression rates of synaptophysin1, vesicle-associated membrane protein1 (VAMP1), vesicle-associated membrane protein2 (VAMP2), synaptotagmin1, synaptophysin1, and synaptic vesicle protein2A (SV2A) were not significantly changed after fasudil treatment (Figure 2b). However, the fact that fasudil is a kinase inhibitor also prompted us to analyze the phosphorylation state of synapsin1, a protein whose behavior is strongly controlled by phosphorylation (Cesca et al., 2010). Synapsin1 phosphorylation at site 6 (Syn1(549)) increased substantially in fasudil-treated cultures (Figure 2b). To determine whether this change affected synapses or other cell compartments, we analyzed pSyn1(549) in

the pre-synaptic compartment of stimulated and unstimulated cultures. An increase in the phosphorylated synapsin1 was found in synapses, as in Figure 2b (Figure 2d and e), but it was limited in amplitude, and not statistically significant. As expected from the literature (Cesca et al., 2010), stimulation increased the phosphorylated synapsin1 levels (Figure 2e), and this effect was reduced by fasudil substantially (Figure 2e). The investigation of phosphorylation of synapsin1 at site 1 (pSyn1(9)) in stimulated and unstimulated neurons resulted in no significant changes after fasudil treatment (data not shown).

This implies that, while fasudil does not induce strong overall changes in synaptic protein abundance, it may result in more subtle functional changes, for example by modulating protein phosphorylation. Finally, the lack of an overall effect of fasudil on synapses was confirmed by the fact that no substantial changes in the number of synapses could be detected (Figure 2c), in line with the similar observations we made for the synapse morphology (Figure 1).

3.3 | The recycling pool is strongly reduced after chronic ROCK inhibition

The synapsins and their phosphorylation are strongly involved in tethering the synaptic vesicles to the actin cytoskeleton and to each other, in a process that is thought to have important effects in the regulation of the active-recycling and reserve pools of synaptic vesicles (Cesca et al., 2010; Rizzoli, 2014; Song & Augustine, 2015). Having found a significant difference in synapsin1 phosphorylation at site 6 upon fasudil treatment, we sought to analyze vesicle pool dynamics in these cultures.

A frequently used procedure is the application of physiological stimulus trains to induce synaptic vesicle recycling. The vesicles are then detected by different fluorescence-based tools, and the vesicle pools sizes, as well as their dynamics, can be reported. We first employed an assay based on a fluorescently conjugated antibody directed against the intravesicular domain of the synaptic vesicle calcium sensor synaptotagmin1 (Syt1). This epitope is exposed during exocytosis, and the antibodies that detect it become endocytosed, and therefore are labeled fluorescently. We first stimulated neurons, in the presence of Atto647N-conjugated Syt1 antibodies, for 30 s, at 20 Hz, a strong physiological stimulus that labels the entire actively recycling pool of synaptic vesicles (Truckenbrodt et al., 2018). Afterward the cultures were fixed and immunostained for the synaptic vesicle marker synaptophysin1 (Syp1), to enable the precise identification of synaptic boutons (Figure 3a).

A negative control for the stimulation procedure was generated by incubating the cells in the presence of the sodium channel blocker tetrodotoxin (TTX), which inhibits network activity. The antibodies in this case only detect the surface pool of Syt1 molecules (Figure 3a), which here makes up about 13% of all Syt1 molecules, identified with a total stain (total stain mean normalized to Syt1 surface: 8.03 ± 0.34 SEM, $n = 45$ analyzed regions with hundreds of synapses analyzed from 1 cell culture preparation). A comparison of the signals obtained in the presence or in the absence of stimulation provides a precise estimate of the size of the vesicle population that responds to stimulation (the recycling pool). A quantification of the Syt1 intensity in the synapses revealed that fasudil treatment increased the surface population of Syt1 by ~ 35% (Figure 3b), while also reducing the population of vesicles that responded to stimulation (Figure 3c).

3.4 | The kinetics of synaptic exo- and endocytosis are not altered after fasudil treatment

To further study the vesicle behavior of the synaptic vesicles, we relied on a variant of the Syt1 antibody assay, in which the fluorophore employed is pH-sensitive, to exploit the difference between the neutral pH of the external milieu and the acidic pH of the vesicles. We pre-incubated the cultures with the Syt1 antibodies conjugated to the pH-sensitive dye CypHer5E, for 1 hr. This treatment is sufficient for the complete labeling of the recycling pool, whose vesicles exo- and endocytose repeatedly, because of the high levels of spontaneous network activity in the cultures (Truckenbrodt et al., 2018). The cultures can then be stimulated, as performed above. During stimulation, the vesicles exocytose, thereby bringing CypHer5E in contact with the neutral pH, which quenches the dye. During endocytosis the vesicles become acidified, which un-quenches the dye, thereby allowing us to investigate both exo- and endocytosis dynamics.

We recorded the CypHer5E fluorescence during and after 20 Hz/ 30 s stimulus trains (Figure 4). Neither the signals observed during stimulation (reflecting mostly exocytosis), neither those observed after stimulation (reflecting mostly endocytosis) showed any differences between fasudil-treated and control cultures, enabling us to conclude that this treatment does not change the kinetics of exo- or endocytosis.

These results imply that, although fewer actively recycling vesicles are employed (Figure 3), their recycling kinetics are not significantly affected by the fasudil treatment.

3.5 | Fasudil-treated neurons show normal calcium signaling during stimulation

To identify the mechanisms that lead to lower numbers of recycling vesicles after electrical stimulation, we first focused on the general activity of neurons. In principle, a conceivable explanation for the reduced numbers of vesicles released upon stimulation (Figure 3) is a reduction in calcium signaling at synapses.

To test this, cells were co-transfected with the calcium sensor GCaMP6s and with the vesicle recycling sensor SypHy (Chen et al., 2013; Truckenbrodt et al., 2018). The latter was used as an indicator for the position of synaptic boutons, which cannot be derived solely from the GCaMP6s images. Spontaneous, as well as stimulated synaptic activity were then analyzed in synaptic boutons by measuring the fluorescence intensity of GCaMP6s (Figure 5). We
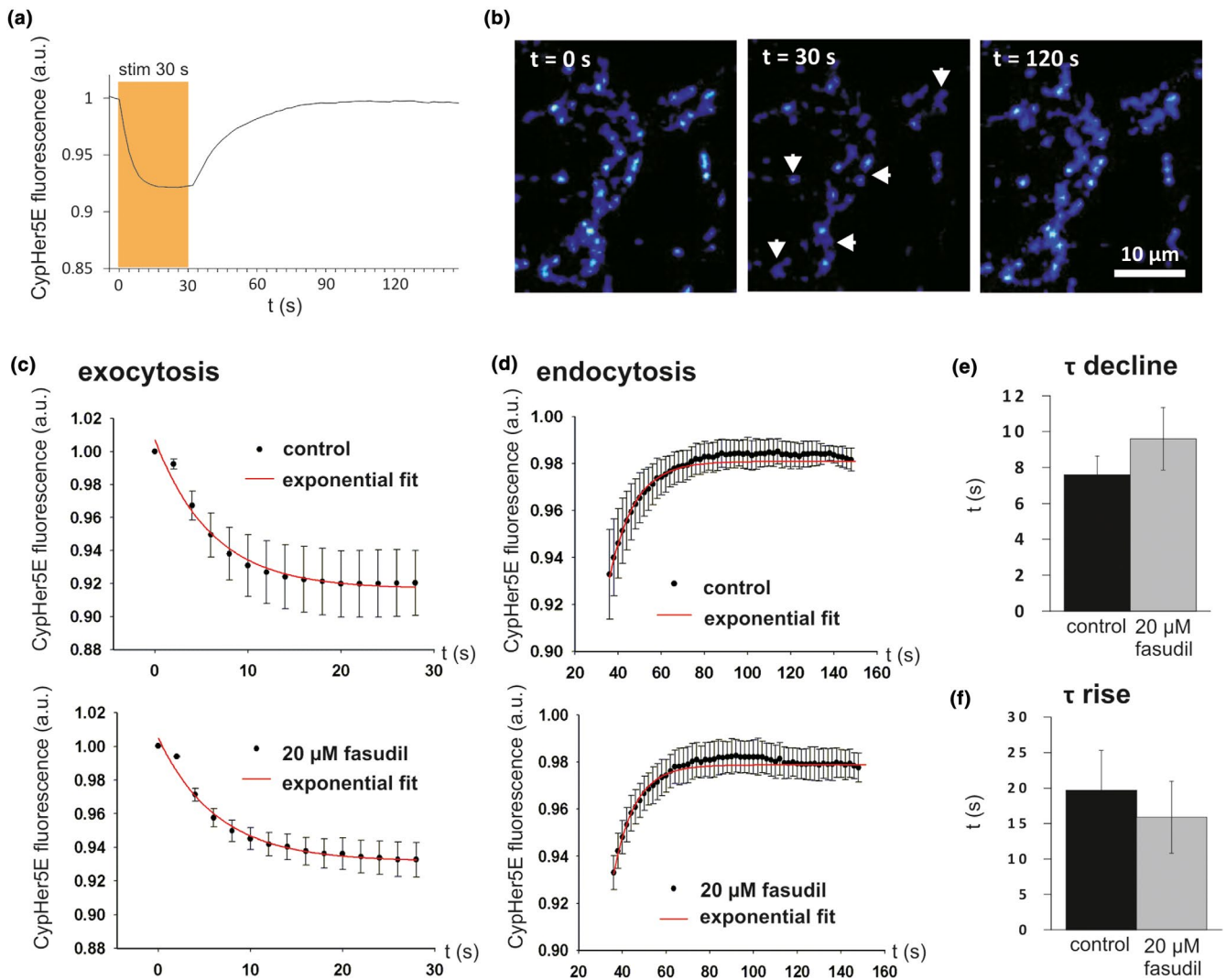
FIGURE 4 Analysis of synaptic vesicle exo- and endocytosis kinetics after fasudil treatment. (a) Syt1 antibodies conjugated to the pH-sensitive dye CypHer5E. The dye is highly fluorescent in the acidic interior of the vesicles, becomes quenched as they exocytose and it is exposed to the neutral pH of the extracellular buffer, and is again fluorescent after endocytosis and re-acidification. The curve shows the outline of the experiment: stimulation for 30 s at 20 Hz is followed by 150 s of imaging, to enable the vesicles to endocytose and re-acidify. (b) Three representative images from controls are shown, before ($t = 0$ s), during ($t = 30$ s) and after ($t = 120$ s) stimulation. The white arrowheads point on regions of interest which are changing in fluorescence during stimulation. (c) Average CypHer5E curves depicting the response to stimulation from 20 control neurons (top) or 18 fasudil-treated neurons (bottom) both obtained from 3 independent cell culture preparations. Exponential fits were used to determine the time constant (τ) of exocytosis. (d) Similar curves for the recovery of the signal after the end of stimulation (15 and 10 neurons, respectively, both obtained from 3 independent cell culture preparations). (e–f) An analysis of the time constants for exo- or endocytosis. No significant differences between fasudil-treated and control cultures could be detected with Mann-Whitney-test in E and student´s t-test in F. Data are presented as individual data points and mean $\pm$ SEM

imaged the neurons first without external stimulation, for 60 s, to record the spontaneous network activity of the cultures. The mean number of spontaneous spikes amounted to 2.1 spikes/minute for control neurons, and 2.4 spikes/ minute for fasudil-treated cells, with a range of values of 0 to 7 spikes per minute, for both conditions. Thus, no significant difference could be detected.

We then applied three stimulation trains, of increasing length, at 20 Hz (1 s, 10 s, and 50 s). All trains elicited strong GCaMP6s fluorescence changes (Figure 5a), which were virtually identical in fasudil-treated cells and in controls. Neither the peak Ca^{2+} signals (Figure 5b), nor the total signals (Figure 5c) were significantly

different in the fasudil-treated samples, suggesting that this drug leaves Ca^{2+} signaling in synapses unaffected.

3.6 | Fasudil-treated neurons show a faster synaptic vesicle turnover

The results presented above suggest that the synaptic vesicle recycling kinetics are not affected by fasudil, which also leaves Ca^{2+} signaling unaffected. One further potential explanation for the differences in synaptic vesicle pools observed in Figure 3 was suggested by a published
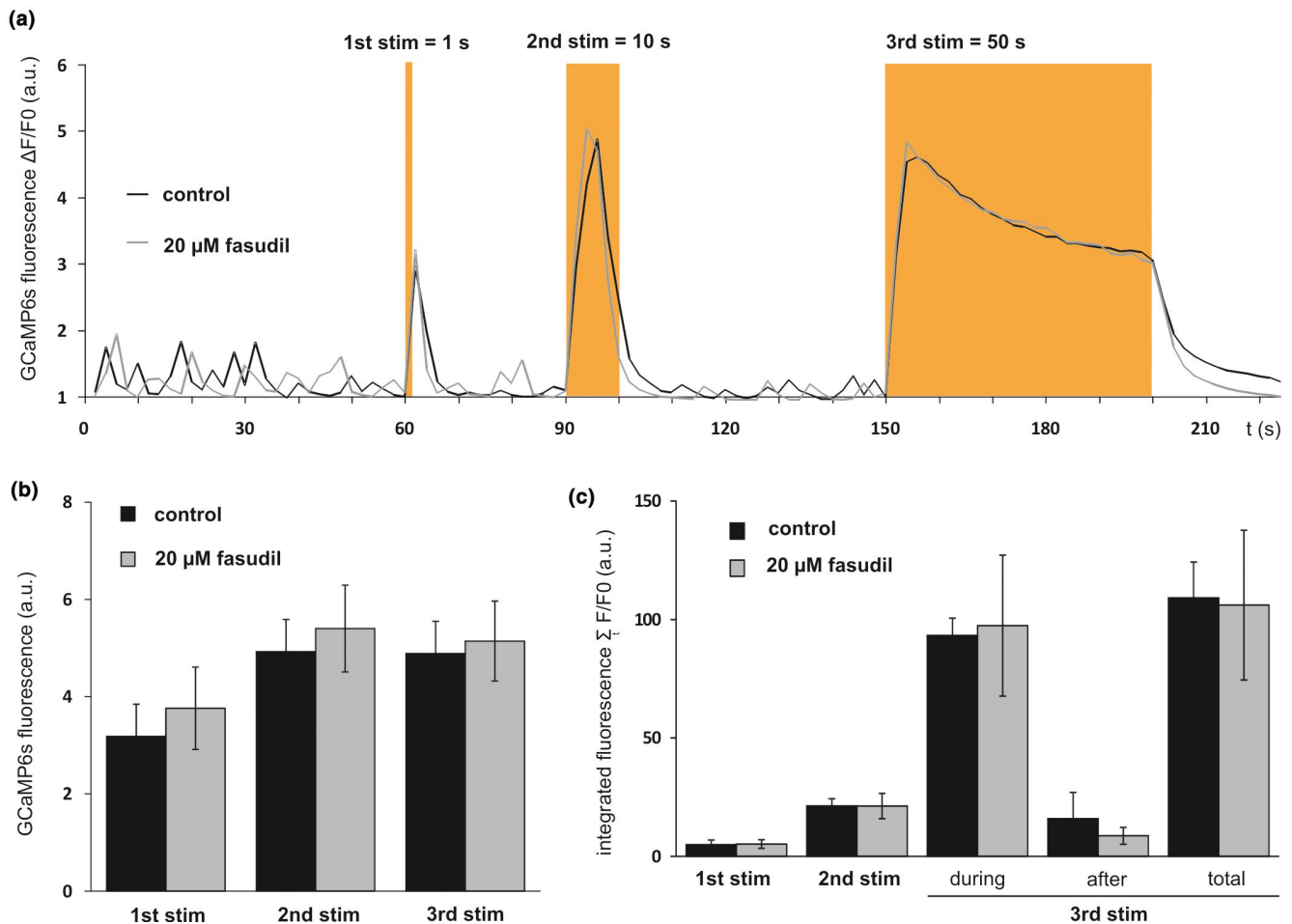
FIGURE 5 Fasudil does not affect Ca2+ signaling in synapses. (a) The traces indicate GCaMP6s. fluorescence in synaptic boutons (identified relying on SypHy fluorescence), in controls or in fasudil-treated samples. The temporal positions and the lengths of three stimulation trains are indicated. (b) An analysis of the peak fluorescence intensity upon stimulation. No significant differences could be detected. (c) An analysis of the cumulative fluorescence intensity, from the same traces as in (b). Again, no significant differences could be detected. Data are presented as individual data points and mean $\pm$ SEM from $n = 3$ independent culture preparations with several hundred synapses analyzed per experiment

analysis of the synaptic vesicle turnover (Truckenbrodt et al., 2018). When synaptic vesicles become older, they are reluctant to release, which results in a reduction of the recycling pool. This is paralleled by an increase in the surface pool of vesicle molecules, since the old vesicles are more poorly endocytosed (Truckenbrodt et al., 2018). Therefore, a conceivable explanation of the results observed so far would be that fasudil accelerates the turnover of the vesicles, and thereby presumably forces the neurons to employ older vesicles in synaptic transmission more often than in control neurons.

To test this, we relied again on a variant of the Syt1 antibody assay. An Atto647N-conjugated Syt1 antibody was added to the cells on DIV11 (after one day of fasudil treatment), and was incubated with the cultures for 1 hr at 37°C, which results in the labeling of the entire recycling pool, as mentioned above. The cells are then investigated at multiple days after labeling (Figure 6a). The loss of signal from the synapses is a direct indication of vesicle turnover (Truckenbrodt et al., 2018). The signal decreased in both fasudil-treated neurons and in their controls (Figure 6b), but the loss

was significantly more rapid in fasudil-treated neurons (Figure 6c). This suggests that chronic fasudil treatment enhances the rate of synaptic vesicle degradation, thereby accelerating their turnover.

4 | DISCUSSION

The search for disease-modifying treatments that support neuronal restoration is one of the main interests of current neuroscience research. Treatment strategies should aim at prevention of neuronal death and at restoration of function in the remaining population. One promising strategy is the regulation of the Rho-kinase (ROCK) signaling pathway. Its activation is followed by growth cone collapse and neurite retraction (Amano et al., 1997), while its inhibition supports neuronal growth and the activation of survival cascades (Koch et al., 2014; Saal et al., 2015). The pharmacological ROCK inhibitor fasudil was shown to specifically inhibit ROCK1 and ROCK2, although it also affects other kinases with lower affinity (Davies
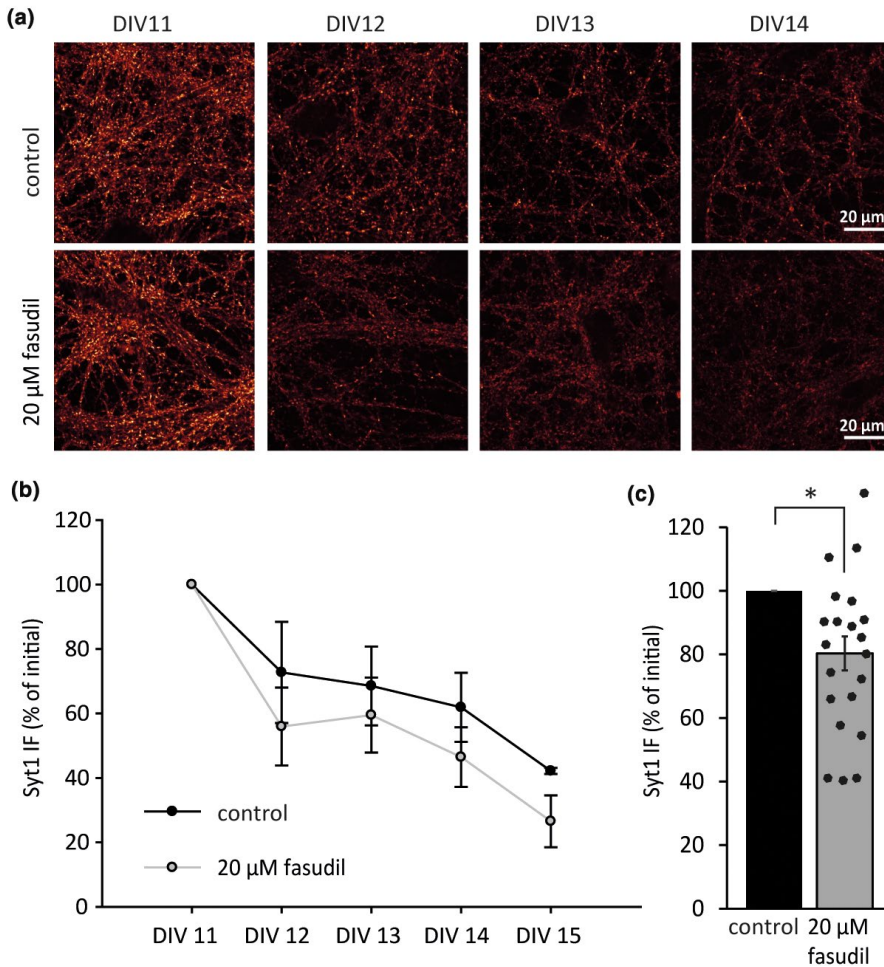
FIGURE 6 Fasudil accelerates synaptic vesicle turnover. (A) Synaptic vesicles were labeled with fluorescently-conjugated Syt1 antibodies, and were imaged immediately, or at several days after labeling. The signal loss indicates the degradation of the labeled vesicles. (b) Fluorescence quantification. Data are presented as mean ± SD, with n = 7 (DIV11 to DIV13), n = 5 (DIV14) and n = 2 (DIV15) independent cell culture preparations with several hundred synapses analyzed per experiment. (c) The intensity values of the fasudil-treated experiments were normalized to their respective controls and the effect of fasudil was determined between DIV12 and DIV15. Data is depicted here as individual data points and/or mean ± SEM. *p < .05 (paired student's t-test)

et al., 2000; Feng et al., 2016). It is well tolerated in the treatment of human cerebral and coronary vasospasms (Kikuchi et al., 2019; Shibuya et al., 1992), and results in attenuated cell death, upregulation of survival-promoting cascades, and promotes the regenerative capacity in multiple cell and animal models (Takata et al., 2013; Tatenhorst et al., 2014).

Since previous studies only investigated short-time effects of ROCK inhibitors on synaptic transmission (Gonzalez-Forero et al., 2012) or chronic influence on synaptic plasticity (Chen et al., 2015), in this study we investigated the chronic effects of fasudil treatment on the hippocampal pre-synaptic compartment. After 5 days of 20 μm fasudil treatment, the neurons showed a change in the overall actin cytoskeleton, which was visualized by a decreased F-actin proportion (Figure 1a). Also in the pre-synaptic bouton fasudil reduces the filamentous structure of actin, which seems not to be changed for the exocytosis of vesicles after stimulation (Figure 1d and e). These findings are in line with the fact that ROCK inhibition increases cofilin activity via attenuated LIM domain kinase activity, which in turn is followed by actin disassembly and a reduction of stable actin filaments (F-actin), increasing the fluidity of the cytoskeleton (Amano et al., 2010; Endo et al., 2003; Ohashi et al., 2000). In this study, we detected only very little phosphorylated cofilin in the pre-synaptic compartment (Figure 2d), however,

the quantitative analysis of the extrasynaptic pCofilin fluorescence confirmed the enhanced activity of this molecule after chronic fasudil treatment (Figure 2e). The same is true for phospho-myosin regulatory light chain, which regulates actin-myosin interactions in a ROCK-dependent manner (Schröter et al., 2008). As expected, ROCK inhibition leads to a pronounced decrease in phosphorylated MRLC in the stimulated pre-synapse (Figure 2d and e), however, most of the protein is localized in other cell parts. While it is still not clear how the actin cytoskeleton is involved in vesicle release, we can nevertheless conclude that chronic ROCK inhibition via fasudil affects its filamentous structure, while it does not affect profoundly synapse morphology or the arrangement of actin in the synapse (Figure 1b and c).

To further characterize the fasudil effect on the pre-synaptic composition, we used western blot analyses to quantify synaptic vesicle-related proteins. No changes could be detected in the abundance of six different relevant synaptic proteins (Figure 2). Since fasudil is a kinase inhibitor, we tested the phosphorylation level of synapsin1, especially because synapsin1 is known to be directly linked to actin (Bloom et al., 2002; Cingolani and Goda, 2008), and to thus tether the synaptic vesicles to the actin cytoskeleton (Ceccaldi et al., 1995; Chi et al., 2003). The phosphorylation of this protein releases the vesicles and promotes their integration to the recycling

pool. Interestingly, here we measured an increase in phosphorylated synapsin1 at its D domain (Ser549) after chronic fasudil treatment (Figure 2a and b). This domain is under a complex regulation, being phosphorylated by both mitogen-activated protein kinase (MAPK) and Cdk5 (Cyclin-dependent kinase 5) (Cesca et al., 2010; Song & Augustine, 2015), thereby leading either to the dissociation from the synaptic vesicle membrane or to the detachment of the actin cytoskeleton (Chi et al., 2003). In principle, this would release synaptic vesicles from the synapsin-bound state.

The synapsin-bound vesicles are classically thought to be a major part of the so-called reserve pool of synaptic vesicles (Rizzoli & Betz, 2005). Synaptic vesicles are divided by their behavior in response to stimulation in the following pools: first, the readily releasable pool (RRP), which is thought to comprise the vesicles that are docked to the active zone and are immediately able to exocytose upon mild stimulation (Rizzoli & Betz, 2004). Second, the recycling pool, which provides releasable vesicles following a moderate stimulation, by continuously recycling vesicles. Third, the reserve pool vesicles, which are only mobilized when the recycling pool is depleted by stimuli that surpass the physiological conditions (Richards et al., 2000; Rizzoli, 2014). In principle, higher phosphorylation levels of synapsin1 would reduce the size of the reserve pool, and would increase the fraction of recycling vesicles (Rizzoli, 2014). Our observations conflict with this hypothesis, as we discovered that fasudil reduced significantly the size of the recycling pool (Figure 3), without

affecting the total amount of vesicles or vesicle proteins (Figure 1, Figure 2).

A potential explanation for these observations would be the following. The increased synapsin1 phosphorylation upon fasudil treatment, as observed by western blotting (Figure 2a), probably takes part mostly outside synapses, since synaptic effects are of very small amplitude (Figure 2e). In contrast, a stronger effect of fasudil can be observed in synapses upon stimulation, when fasudil reduces considerably the synapsin1 phosphorylation (Figure 2e). This suggests that fasudil treatment blocks the dissociation of vesicles from the reserve pool, resulting in a smaller recycling pool, as measured in Figure 3.

Consequently, a smaller fraction of synaptic vesicles has to be more often recruited for exocytosis upon stimulation. We have found in the past that such an accelerated usage enhances the aging of the respective vesicles (Truckenbrodt et al., 2018). This renders them less prone to activity, thereby further decreasing the recycling pool (Truckenbrodt et al., 2018). Such a pool would be able to respond to normal stimuli, but would fail to sustain strong stimulation periods, as the smaller recycling pool becomes depleted (summarized in Figure 7).

Such effects of fasudil treatment would be expected to depend strongly on the network activity levels of each culture, which in turn are dependent on the connectivity and the density attained on each coverslip. These effects cannot be reproduced precisely among
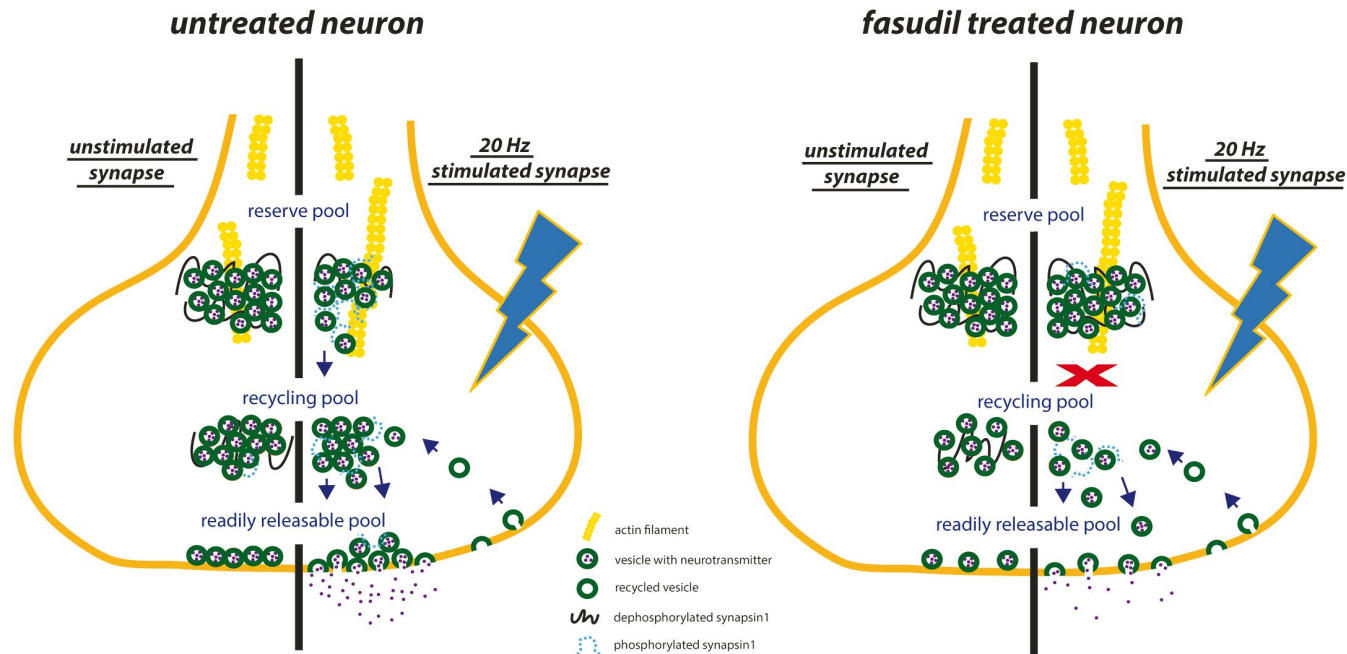

FIGURE 7 Scheme of the effects of chronic fasudil treatment on the synaptic vesicle pool size by modulating synapsin1 phosphorylation. Left: The untreated synapse: The synaptic vesicles are tethered to the actin cytoskeleton in the reserve pool by dephosphorylated synapsin1. The recycling pool and the readily-releasable pool are filled with vesicles waiting to be released upon stimulation. Strong electrical stimuli result in the phosphorylation of synapsin1, and the vesicles dissociate from actin and are transported to the recycling pool, where they can be released into the readily releasable pool. Right: Chronic fasudil treatment. Following an electrical stimulus, phosphorylation of synapsin1 is blocked via fasudil and many synaptic vesicles stay tethered in the reserve pool. Consequently, the recycling pool is diminished. These recycled vesicles have to undergo the release cycle more often than in control and are prone to more rapid degradation, overall further reducing the size of the recycling pool

coverslips, which implies that the speed of the initial effects will be quite variable, and likely cannot be sufficiently quantified with the tools used here. However, a number of other observations are in good agreement with this hypothesis. First, chronic fasudil treatment does not change exo- and endocytosis kinetics, (as shown in Figure 4) contrary to a previous study that reports a slow-down of endocytosis with the ROCK inhibitor Y-27632 in calyces of Held synapses (Taoufiq et al., 2013), Second, there was also no fasudil effect on pre-synaptic activity (Figure 5). The electrical stimulation of fasudil-treated hippocampal neurons triggered the same neuronal Ca^{2+} response as in vehicle-treated cells. Finally, the degradation rate of the vesicles was indeed enhanced (Figure 6).

A small pool of recycling synaptic vesicles would be expected to age faster than a large one, and to be degraded more rapidly. Recent observations suggest that synaptic vesicle aging is directly linked to the amount of cycles of exo- and endocytosis undergone by the respective vesicles (Truckenbrodt et al., 2018). The mechanism may involve the vesicles picking up a contaminant from the plasma membrane, SNAP25, which then interferes with the vesicle ability to exocytose, and primes them for degradation (Truckenbrodt et al., 2018). A smaller recycling pool implies that the same vesicles need to be repeatedly exo- and endocytosed, at higher rates than in synapses which can rely on more synaptic vesicles for this process. This, in turn, would force the over-active vesicles to age faster, and to be degraded faster, as we have observed, according to the contamination hypothesis mentioned above. At the same time, aged vesicles are endocytosed more poorly (Truckenbrodt et al., 2018), which would result in more vesicle material stranded on the surface membrane, as we have also observed (Figure 3).

From this study, we can conclude that the fasudil treatment is not deleterious to pre-synapses and does not change most of their functional parameters. Only during strong stimuli, as those used in Figure 3, it seems to result in a lower number of released vesicles. This observation might be useful in the treatment of particular diseases, where neuronal damage results in accelerated disease progression via glutamate-excitotoxicity. Meziane and colleagues have already shown that chronic fasudil treatment in a mouse model of intellectual disability counteracts hyperactivity orginated from excessively active synapses (Meziane et al., 2016). Strong aberrant signaling from damaged cells strongly stimulates post-synaptic neurons and may result in pathological overactivity, which is known from different synaptopathies: for example, in Parkinson´s disease the neurons of the subthalamic nucleus are overactive because of decreased nigral stimulation. Drugs specifically reducing the ability of synapses to respond to such unusually strong stimuli, while still enabling them to function in normal neuronal firing (Figure 5), could be a clinically useful resource.

Overall, our findings contribute to build a more precise characterization of fasudil, and support the application of this drug that is currently in clinical trials for the treatment of neurodegenerative diseases (Lingor et al., 2019). Further investigations will be needed to fully characterize the effects of this drug on synaptic function in animal models.

CONFLICT OF INTEREST

Mathias Bähr is an editor for the Journal of Neurochemistry. All other authors declare no conflict of interest related to this manuscript.

ORCID

Kim Ann Saal https://orcid.org/0000-0001-9706-3734

REFERENCES

Amano, M., Chihara, K., & Kimura, K. (1997). Formation of actin stress fibers and focal adhesions enhanced by rho-kinase. *Science (80-.,), 275*, 1308–1312. https://doi.org/10.1126/science.275.5304.1308

Amano, M., Nakayama, M., & Kaibuchi, K. (2010). Rho-kinase/ROCK: A key regulator of the cytoskeleton and cell polarity. *Cytoskeleton (Hoboken), 67*, 545–554. https://doi.org/10.1002/cm.20472

Barcia, C., Ros, C. M., Annese, V., Carrillo-de Sauvage, M. A., Ros-Bernal, F., Gómez, A., Yuste, J. E., Campuzano, C. M., de Pablos, V., Fernandez-Villalba, E., & Herrero, M. T. (2012). ROCK/Cdc42-mediated microglial motility and gliapse formation lead to phagocytosis of degenerating dopaminergic neurons in vivo. *Scientific Reports, 2*, 809. https://doi.org/10.1038/srep00809

Bereczki, E., Branca, R. M., Francis, P. T., Pereira, J. B., Baek, J.-H., Hortobágyi, T., Winblad, B., Ballard, C., Lehtiö, J., & Aarsland, D. (2018). Synaptic markers of cognitive decline in neurodegenerative diseases: A proteomic approach. *Brain, 141*(2), 582–595. https://doi.org/10.1093/brain/awx352

Bloom, O., Evergren, E., Tomilin, N., Kjaerulff, O., Löw, P., Brodin, L., Pieribone, V. A., Greengard, P., & Shupliakov, O. (2002). Colocalization of synapsin and actin during synaptic vesicle recycling. *Cell Biol., 161*, 737–747. https://doi.org/10.1083/jcb.200212140

Bowerman, M., Murray, L. M., Boyer, J. G., Anderson, C. L., & Kothary, R. (2012). Fasudil improves survival and promotes skeletal muscle development in a mouse model of spinal muscular atrophy. *BMC Medicine, 10*, 24. https://doi.org/10.1186/1741-7015-10-24

Burke, R. E., & O'Malley, K. (2013). Axon degeneration in Parkinson's disease. *Experimental Neurology, 246*, 72–83. https://doi.org/10.1016/j.expneurol.2012.01.011

Ceccaldi, P. E., Grohovaz, F., Benfenati, F., Chieregatti, E., Greengard, P., & Valtorta, F. (1995). Dephosphorylated synapsin I anchors synaptic vesicles to actin cytoskeleton: An analysis by videomicroscopy. *Journal of Cell Biology, 128*, 905–912. https://doi.org/10.1083/jcb.128.5.905

Cesca, F., Baldelli, P., Valtorta, F., & Benfenati, F. (2010). The synapsins: Key actors of synapse function and plasticity. *Progress in Neurobiology, 91*, 313–348. https://doi.org/10.1016/j.pneurobio.2010.04.006

Chaudhuri, K. R., Healy, D. G., & Schapira, A. H. V. (2006). Non-motor symptoms of Parkinson's disease: Diagnosis and management. *The Lancet Neurology, 5*, 235–245. https://doi.org/10.1016/S1474-4422(06)70373-8

Chen, C., Yu, J. Z., Zhang, Q., Zhao, Y. F., Liu, C. Y., Li, Y. H., Yang, W. F., Ma, C. G., & Xiao, B. G. (2015). Role of rho kinase and fasudil on synaptic plasticity in multiple sclerosis. *NeuroMolecular Medicine, 17*, 454–465. https://doi.org/10.1007/s12017-015-8374-6

Chen, T., Wardill, T. J., Sun, Y., Pulver, S. R., Renninger, S. L., Baohan, A., Schreiter, E. R., Kerr, R. A., Orger, M. B., Jayaraman, V., Looger, L. L., Svoboda, K., & Kim, D. S. (2013). Ultrasensitive fluorescent proteins for imaging neuronal activity. *Nature*, *499*(7458), 295–300. https://doi.org/10.1038/nature12354

Chi, P., Greengard, P., & Ryan, T. A. (2003). Synaptic vesicle mobilization is regulated by distinct synapsin i phosphorylation pathways at different frequencies. *Neuron*, *38*, 69–78. https://doi.org/10.1016/S0896-6273(03)00151-X

Cingolani, L. A, & Goda, Y.(2008). Actin in action: The interplay between the actin cytoskeleton and synaptic efficacy. *Nature Reviews Neuroscience*, *9*, 344–356. https://doi.org/10.1038/nrn2373

Davies, S. P., Reddy, H., Caivano, M., & Cohen, P. (2000). Protein kinase inhibitors. *Journal of Biochemistry*, *351*, 95–105.

Endo, M., Ohashi, K., Sasaki, Y., Goshima, Y., Niwa, R., Uemura, T., & Mizuno, K. (2003). Control of growth cone motility and morphology by LIM kinase and slingshot via phosphorylation and dephosphorylation of cofilin. *The Journal of Neuroscience*, *23*(7), 2527–2537. 23/7/2527[pii].

Feng, Y., Lograsso, P. V., Defert, O., & Li, R. (2016). Rho kinase (ROCK) inhibitors and their therapeutic potential. *Journal of Medicinal Chemistry*, *59*, 2269–2300. https://doi.org/10.1021/acs.jmedchem.5b00683

Gallo, G. (2010). RhoA-kinase coordinates F-actin organization and myosin 2 activity during semaphorin-3A-indiced axon retraction. *Journal of Cell Science*, *119*(PT 16): 3413. https://doi.org/10.1242/jcs.03084

Gonzalez-Forero, D., Montero, F., Garcia-Morales, V., Dominguez, G., Gomez-Perez, L., Garcia-Verdugo, J. M., & Moreno-Lopez, B. (2012). Endogenous rho-kinase signaling maintains synaptic strength by stabilizing the size of the readily releasable pool of synaptic vesicles. *Journal of Neuroscience*, *32*, 68–84. https://doi.org/10.1523/JNEUROSCI.3215-11.2012

Guertin, D. A., & Sabatini, D. M. (2007). Defining the role of mTOR in cancer. *Cancer Cell*, *12*, 9–22. https://doi.org/10.1016/j.ccr.2007.05.008

Günther, R., Saal, K.-A., Suhr, M., Scheer, D., Koch, J. C., Bähr, M., Lingor, P., & Tönges, L. (2014). The rho kinase inhibitor Y-27632 improves motor performance in male SOD1(G93A) mice. *Frontiers in Neuroscience*, *8*, 304. https://doi.org/10.3389/fnins.2014.00304

Henderson, B. W., Gentry, E. G., Rush, T., Troncoso, J. C., Thambisetty, M., Montine, T. J., & Herskowitz, J. H. (2017). Rho-associated protein kinase 1 (ROCK1) is increased in Alzheimer's disease and ROCK1 depletion reduces amyloid-β levels in brain. *Journal of Neurochemistry*, *138*(4), 525–531. https://doi.org/10.1111/jnc.13688

Herskowitz, J. H., Feng, Y., Mattheyses, A. L., Hales, C. M., Higginbotham, L. A., Duong, D. M., Montine, T. J., Troncoso, J. C., Thambisetty, M., Seyfried, N. T., Levey, A. I., & Lah, J. J. (2013). Pharmacologic inhibition of ROCK2 suppresses amyloid-ß production in an Alzheimer's disease mouse model. *Journal of Neuroscience 33*, 19086–19098. https://doi.org/10.1523/JNEUROSCI.2508-13.2013

Kikuchi, Y., Takahashi, J., Hao, K., Sato, K., Sugisawa, J., Tsuchiya, S., Suda, A., Shindo, T., Ikeda, S., Shiroto, T., Matsumoto, Y., Miyata, S., Sakata, Y., & Shimokawa, H. (2019). Usefulness of intracoronary administration of fasudil, a selective Rho-kinase inhibitor, for PCI-related refractory myocardial ischemia. *International Journal of Cardiology*, *297*, 8–13. https://doi.org/10.1016/j.ijcard.2019.09.057

Koch, J. C., Tatenhorst, L., Roser, A.-E., Saal, K.-A., Tönges, L., & Lingor, P. (2018). Pharmacology & Therapeutics ROCK inhibition in models of neurodegeneration and its potential for clinical translation. *Pharmacology & Therapeutics*, *189*, 1–21. https://doi.org/10.1016/j.pharmthera.2018.03.008

Koch, J. C., Tönges, L., Barski, E., Michel, U., Bähr, M., & Lingor, P. (2014). ROCK2 is a major regulator of axonal degeneration, neuronal death and axonal regeneration in the CNS. *Cell Death & Disease*, *5*, 1–12. https://doi.org/10.1038/cddis.2014.191

Komagome, R., Kimura, K., & Saito, M. (2000). Postnatal changes in Rho and Rho-related proteins in the mouse brain. *Japanese Journal of Veterinary Research*, *47*, 127–133.

Lane, R. F., Gatson, J. W., Small, S. A., Ehrlich, M. E., & Gandy, S. (2010). Protein kinase C and rho activated coiled coil protein kinase 2 (ROCK2) modulate Alzheimer 's APP metabolism and phosphorylation of the. *Molecular Neurodegeneration*, *5*, 62. https://doi.org/10.1186/1750-1326-5-62

Lau, C. L., Perreau, V. M., Chen, M. J., Cate, H. S., Merlo, D., Cheung, N. S., O'Shea, R. D., & Beart, P. M. (2012). Transcriptomic profiling of astrocytes treated with the Rho kinase inhibitor fasudil reveals cytoskeletal and pro-survival responses. *Journal of Cellular Physiology*, *227*, 1199–1211. https://doi.org/10.1002/jcp.22838

Lee, H. M., & Koh, S. (2015). Many faces of Parkinson's disease: Symptoms of Parkinson's disease. *Journal of Movement Disorders 8*, 92–97.

Lingor, P., Teusch, N., Schwarz, K., Mueller, R., Mack, H., Bähr, M., & Mueller, B. K. (2007). Inhibition of Rho kinase (ROCK) increases neurite outgrowth on chondroitin sulphate proteoglycan in vitro and axonal regeneration in the adult optic nerve in vivo. *Journal of Neurochemistry*, *103*, 181–189. https://doi.org/10.1111/j.1471-4159.2007.04756.x

Lingor, P., Weber, M., Camu, W., Friede, T., Hilgers, R., Leha, A., Neuwirth, C., Günther, R., Benatar, M., Kuzma-Kozakiewicz, M., Bidner, H., Blankenstein, C., Frontini, R., Ludolph, A., & Koch, J. C. (2019). ROCK-ALS: Protocol for a double-blind phase iia trial of safety, tolerability and efficacy of the rho kinase (ROCK) inhibitor fasudil in amyotrophic lateral sclerosis. *Frontiers in Neurology*, *10*, 1–11. https://doi.org/10.3389/fneur.2019.00293

Meziane, H., Khelfaoui, M., Morello, N., Hiba, B., Calcagno, E., Reibel-Foisset, S., Selloum, M., Chelly, J., Humeau, Y., Riet, F., Zanni, G., Herault, Y., Bienvenu, T., Giustetto, M., & Billuart, P. (2016). Fasudil treatment in adult reverses behavioural changes and brain ventricular enlargement in Oligophrenin-1 mouse model of intellectual disability. *Human Molecular Genetics*, *25*, 2314–2323. https://doi.org/10.1093/hmg/ddw102

Monnier, P. P., Sierra, A., Schwab, J. M., Henke-Fahle, S., & Mueller, B. K. (2003). The Rho/ROCK pathway mediates neurite growth-inhibitory activity associated with the chondroitin sulfate proteoglycans of the CNS glial scar. *Molecular and Cellular Neurosciences*, *22*, 319–330. https://doi.org/10.1016/S1044-7431(02)00035-0

Morales, M., Colicos, M. A., & Goda, Y. (2000). Actin-dependent regulation of neurotransmitter release at central synapses. *Neuron*, *27*, 539–550. https://doi.org/10.1016/S0896-6273(00)00064-7

Mueller, B. K., Mack, H., & Teusch, N. (2005). Rho kinase, a promising drug target for neurological disorders. *Nature Reviews Drug Discovery*, *4*, 387–398. https://doi.org/10.1038/nrd1719

Ohashi, K., Nagata, K., Maekawa, M., Ishizaki, T., Narumiya, S., & Mizuno, K. (2000). Rho-associated Kinase ROCK Activates LIM-kinase 1 by Phosphorylation at Threonine 508 within the Activation Loop *. *Journal of Biological Chemistry*, *275*, 3577–3582. https://doi.org/10.1074/jbc.275.5.3577

Opazo, F., Punge, A., Bückers, J., Hoopmann, P., Kastrup, L., Hell, S. W., & Rizzoli, S. O. (2010). Limited intermixing of synaptic vesicle components upon vesicle recycling. *Traffic*, *11*, 800–812. https://doi.org/10.1111/j.1600-0854.2010.01058.x

Park, J., Arakawa-Takeuchi, S., Jinno, S., & Okayama, H. (2011). Rho-associated kinase connects a cell cycle-controlling anchorage signal to the mammalian target of rapamycin pathway. *Journal of Biological Chemistry*, *286*, 23132–23141. https://doi.org/10.1074/jbc.M110.209114

Pienaar, I. S., Burn, D., Morris, C., & Dexter, D. (2012). Synaptic protein alterations in Parkinson's disease. *Molecular Neurobiology*, *45*, 126–143. https://doi.org/10.1007/s12035-011-8226-9

Richards, D. A., Guatimosim, C., & Betz, W. J. (2000). Two endocytic recycling routes selectively fill two vesicle pools in frog motor nerve terminals. *Neuron*, *27*, 551–559. https://doi.org/10.1016/S0896-6273(00)00065-9

Rizzoli, S. O. (2014). Synaptic vesicle recycling: Steps and principles. *EMBO Journal*, *33*, 788–822. https://doi.org/10.1002/embj.201386357

Rizzoli, S. O., & Betz, W. J. (2004). The structural organization of the readily releasable pool of synaptic vesicles. *Science*, *303*, 2037–2039. https://doi.org/10.1126/science.1094682

Rizzoli, S. O., & Betz, W. J. (2005). Synaptic vesicle pools. *Nature Reviews Neuroscience*, *6*, 57–69. https://doi.org/10.1038/nrn1583

Saal, K.-A., Galter, D., Roeber, S., Bähr, M., Tönges, L., & Lingor, P. (2016). Altered expression of growth associated protein-43 and rho kinase in human patients with Parkinson's disease. *Brain Pathology*, *27*(1), 13–25. https://doi.org/10.1111/bpa.12346

Saal, K.-A., Koch, J. C., Tatenhorst, L., Szegő, E. M., Ribas, V. T., Michel, U., Bähr, M., Tönges, L., & Lingor, P. (2015). AAV.shRNA-mediated downregulation of ROCK2 attenuates degeneration of dopaminergic neurons in toxin-induced models of Parkinson's disease in vitro and in vivo. *Neurobiology of Diseases*, *73*, 150–162. https://doi.org/10.1016/j.nbd.2014.09.013

Sakaba, T., & Neher, E. (2003). Involvement of actin polymerization in vesicle recruitment at the calyx of held synapse. *Journal of Neuroscience*, *23*, 837–846. https://doi.org/10.1523/JNEUROSCI.23-03-00837.2003

Schröter, T., Griffin, E., Weiser, A., Feng, Y., & Lograsso, P. (2008). Biochemical and biophysical research communications detection of myosin light chain phosphorylation — A cell-based assay for screening Rho-kinase inhibitors. *Biochemical and Biophysical Research Communications*, *374*, 356–360. https://doi.org/10.1016/j.bbrc.2008.07.028

Schulz-Schaeffer, W. (2010). The synaptic pathology of a-synuclein aggregation in dementia with Lewy bodies, Parkinson's disease and Parkinson's disease dementia. *Acta Neuropathologica*, *120*, 131–143. https://doi.org/10.1007/s00401-010-0711-0

Shibuya, M., Suzuki, Y., Sugita, K., Saito, I., Sasaki, T., Takakura, K., Nagata, I., Kikuchi, H., Takemae, T., Hidaka, H., & Nakashima, M. (1992). Effect of AT877 on cerebral vasospasm after aneurysmal subarachnoid hemorrhage. *Journal of Neurosurgery*, *76*, 571–577. https://doi.org/10.3171/jns.1992.76.4.0571

Shimokawa, H., Hiramori, K., Iinuma, H., Hosoda, S., Kishida, H., Osada, H., Katagiri, T., Yamauchi, K., Yui, Y., Minamino, T., Nakashima, M., & Kato, K. (2002). Anti-anginal effect of fasudil, a rho-kinase inhibitor, in patients with stable effort angina: A multicenter study. *Journal of Cardiovascular Pharmacology*, *40*, 751–761. https://doi.org/10.1097/00005344-200211000-00013

Song, S., & Augustine, G. J. (2015). Synapsin isoforms and synaptic vesicle trafficking. *Molecules and Cells*, *38*, 936–940.

Spronsen, M. Van, & Hoogenraad, C. C. (2010). Synapse pathology in psychiatric and neurologic disease. *Current Neurology and Neuroscience Reports*, *10*(3), 207–214. 10.1007/s11910-010-0104-8.

Takata, M., Tanaka, H., Kimura, M., Nagahara, Y., Tanaka, K., Kawasaki, K., Seto, M., Tsuruma, K., Shimazawa, M., & Hara, H. (2013). Fasudil, a rho kinase inhibitor, limits motor neuron loss in experimental models of amyotrophic lateral sclerosis. *British Journal of Pharmacology*, *170*, 341–351. https://doi.org/10.1111/bph.12277

Taoufiq, Z., Eguchi, K., & Takahashi, T. (2013). Rho-kinase accelerates synaptic vesicle endocytosis by linking cyclic GMP-dependent protein kinase activity to phosphatidylinositol-4,5-bisphosphate synthesis. *Journal of Neuroscience*, *33*, 12099–12104. https://doi.org/10.1523/JNEUROSCI.0730-13.2013

Tatenhorst, L., Tönges, L., Saal, K.-A., Koch, J. C., Szegő, E. M., Bähr, M., & Lingor, P. (2014). Rho kinase inhibition by fasudil in the striatal 6-Hydroxydopamine lesion mouse model of Parkinson disease. *Journal of Neuropathology & Experimental Neurology*, *73*, 1–10. https://doi.org/10.1097/NEN.0000000000000095

Tönges, L., Frank, T., Tatenhorst, L., Saal, K.-A., Koch, J. C., Szego, É. M., Bähr, M., Weishaupt, J. H., & Lingor, P. (2012). Inhibition of rho kinase enhances survival of dopaminergic neurons and attenuates axonal loss in a mouse model of Parkinson's disease. *Brain*, *135*, 3355–3370. https://doi.org/10.1093/brain/aws254

Tönges, L., Koch, J.-C., Bähr, M., & Lingor, P. (2011). ROCKing regeneration: Rho kinase inhibition as molecular target for neurorestoration. *Frontiers in Molecular Neuroscience*, *4*, 39. https://doi.org/10.3389/fnmol.2011.00039

Truckenbrodt, S., Viplav, A., Jähne, S., Vogts, A., Wildhagen, H., Fornasiero, E. F., Rizzoli, S. O., & Denker, A. (2018). Newly produced synaptic vesicle proteins are preferentially used in synaptic transmission. *EMBO Journal*, *37*, 1–24. https://doi.org/10.15252/embj.201798044

Wishart, T. M., Parson, S. H., & Gillingwater, T. H. (2006). Synaptic vulnerability in neurodegenerative disease. *Journal of Neuropathology & Experimental Neurology*, *65*(8), 733–739. https://doi.org/10.1097/01.jnen.0000228202.35163.c4